DEVELOPMENT OF A PROTOTYPE THREE–FINGER TELEROBOTIC HAND WITH FORCE FEEDBACK FOR GRASPING MULTIFORM OBJECTS

Olorunmotito Noah Femi[a,b]*, Afolayan Matthew Olatunde[a], Alim Sabur Ajibola[a], Yusuf Olatunbosun Tafa[b], Idohen Efemenah Endurance[c]

[a]Mechanical Engineering Department, Ahmadu Bello University, Zaria, Nigeria.
[b]Engineering and Space Systems Department, National Space Research and Development Agency, Abuja, Nigeria.
[c]Department of Agricultural and Biosystems Engineering, University of Kassel, Germany.

*Corresponding email: noahmotito@gmail.com

Article history
Received
6th June 2025
Revised
12th September 2025
Accepted
18th September 2025
Published
1st December 2025

ABSTRACT

Advancement in telerobotic systems is driven by the need to access hazardous environments, the demand for adaptability in dynamically changing conditions, and the desire for enhanced precision in remote operations. These factors necessitate the deployment of highly dexterous robotic hands for mechanical tasks, with humans in the loop for high-level planning and decision-making. Despite their potential in healthcare, manufacturing, space, disaster response, and agriculture, widespread adoption of telerobotic hands is limited by high costs, restricted motion, and control challenges. To address this, a prototype low-cost, 3D-printed, three-finger telerobotic hand was developed. The development process began with the conceptual design of the hand's mechanical structure, followed by design theories to determine finger length, grasping capability, load-carrying capacity, and power requirements. A 3D CAD model was created using SolidWorks and fabricated with a 3D printer, while circuit layout of the components was developed in Fritzing. The assembled components were integrated with electronic modules and programmed in the Arduino IDE to receive servomotors control signals from a joystick-based wireless controller and transmit force-sensitive resistor (FSR) force signals to the robotic hand via Bluetooth communication. The wireless controller itself was designed for ergonomic use. It features adjustable joysticks positions for different hand sizes, signal mapping strategies, and micro-vibration motors for haptic feedback. The platform for its hardware assembly was modeled in SolidWorks and fabricated via 3D printing. The circuit layout of the components was developed in Fritzing. The assembled components were integrated with electronic modules and programmed in the Arduino IDE to transmit servomotors control signals to the robot hand and receive micro-vibration motors control signals generated from FSRs via Bluetooth communication. The hand supports four distinct ranges of motion, namely flexion, extension, abduction, and adduction, and includes fingertip FSRs to measure the force exerted on objects. Experimental results show the telerobotic hand effectively replicated human thumb, index, and middle finger movements as controlled by the joysticks. The system achieved 96.2% motion accuracy resulting from flexion (99.1%), abduction (95%), and adduction (94.5%), with minimal deviation. It attained an 87% grasping success rate with an average grasp time of 2.17 seconds. A positive correlation between measured force and vibration intensity validated the haptic feedback's effectiveness. User feedback indicated an 84% average satisfaction across responsiveness, ease of use, comfort, haptic feedback, fatigue, and task completion. The

prototype successfully demonstrated its ability to replicate human finger motions and provide intuitive control with meaningful force feedback.

Keywords: *Telerobotics, Force sensing and force feedback, Joystick-based Controller, Abduction-Adduction Motion, Multiform object handling*

1.0 INTRODUCTION

Over the past decades, significant progress has been made in the development of telerobotic hands. As is the case with any telerobotic system, this advancement is driven by three key factors: the need to access hazardous environments, the demand for adaptability in dynamically changing environments, and the desire for enhanced precision in remote operations [1, 2]. These factors necessitate the deployment of highly dexterous robotic hands to perform mechanical operations [3], while human operators form part of the control loop, enabling high-level planning and cognitive decision-making [4].

Telerobotic hands offer significant potential across various sectors. In the medical field, the Tele-Robotic Intelligent Nursing Assistant (TRINA), which consists of robotic arms for operation and remote haptic devices for control, has been designed to assist healthcare workers with routine patient care tasks and the management of contaminated materials and protective gear. The system has successfully performed 60% of nursing tasks [5]. During the Fukushima nuclear disaster, remotely operated robotic hands were pivotal in reducing human radiation exposure while performing critical tasks, such as manipulating debris and controlling valves, underscoring their value in disaster response scenarios [6]. In space exploration, telerobotic hands have enabled precision operations such as satellite maintenance and the collection of extraterrestrial samples from Mars, showcasing their potential to operate in harsh extraterrestrial conditions [7]. Similarly, in agriculture, advanced telerobotic hands have enhanced efficiency in fruit harvesting, reducing waste and addressing labor shortages, with the agricultural robotics market projected to reach $20 billion by 2028 [8].

However, despite these advancements, the widespread adoption of telerobotic hands is hindered by several key factors. First, high procurement and maintenance costs – particularly in low- and middle-income countries [9, 10]. For instance, the Shadow Dexterous Hand, a leading product in the market with 20 degrees of freedom, costs about $115,000 [11]. In Nigeria, such a high cost makes robotic manipulation largely inaccessible due to unfavorable exchange rates. Second, limited motion capabilities – specifically the absence of abduction and adduction – restrict the ability of robotic hands to efficiently manipulate irregularly shaped objects [12]. Third, challenges arising from the control techniques adopted. For example, glove-based controllers face issues such as calibration drift, hygiene concerns, and user fatigue [13], while vision-based controllers suffer from high computational requirements, sensitivity to lighting conditions, and latency, all of which reduce their reliability in dynamic environments [14, 15].

Numerous studies have focused on developing telerobotic hands. Puruhita et al. [16] developed a wireless teleoperated humanoid robotic hand controlled using a sensorial glove embedded with flex sensors. Experimental testing demonstrated that the system achieved an average finger tracking error of 2.83%, indicating relatively high accuracy in replicating human hand gestures. However, the system lacked force feedback and was restricted to flexion and extension motions. Bhandari et al. [17] developed a 17-degree-of-freedom (DOF) robotic hand controlled via a wireless glove-based system. Experimental tests showed that the system responded quickly to hand gestures. However, the system relied on predefined gesture mappings and also lacked haptic feedback. Yamakawa et al. [18] developed a high-speed, low-latency telemanipulated three-finger robotic hand system that

utilized non-contact 3D vision-based sensing to track human hand movements and map them to a robotic hand in real time. The system achieved an ultra-low latency of ≤ 20 ms. However, despite its high speed and accuracy, the system relied solely on vision-based tracking, which, while effective, could suffer from occlusion issues and environmental lighting conditions. Additionally, the study did not incorporate haptic feedback.

Fu et al. [19] investigated the teleoperation control of an underactuated bionic hand, comparing wearable glove-based control with vision-tracking-based control using potentiometers and a Leap Motion sensor, respectively. Experimental results showed that the glove-based method achieved higher accuracy (98.6%) but required more physical effort, whereas the vision-based method was less precise (96.5%) but provided a more comfortable user experience. However, the study did not incorporate haptic feedback and also lacked abduction-adduction motions. Coppola et al. [20] developed an affordable teleoperation system for dexterous robotic hands, integrating Leap Motion for hand tracking and a vibrotactile glove for haptic feedback. The results showed that vibrotactile feedback significantly improved grasping success rates, particularly for small and mid-sized objects, and reduced cognitive effort during manipulation tasks. However, the Leap Motion sensor exhibited occasional tracking inconsistencies, which affected real-time motion replication, and the study was based on a simulation rather than real-world robotic execution.

Zhang and Qian [21] developed a wearable teleoperation system integrating a 2-DoF robotic arm, haptic sensors, and a Unity-powered virtual reality (VR) environment for enhanced interaction with virtual objects. The system allowed users to feel force direction, weight perception, and shape rendering through force feedback sensors, achieving 87.3% accuracy in force direction identification. A user study validated its effectiveness in simulating grasping and object manipulation. However, the system was limited to virtual object interaction and required VR equipment, making it less applicable for real-world teleoperation. Al Qaradagi et al. [22] developed a simple, efficient, and cost-effective 3D-printed robotic hand controlled wirelessly via a flex sensor-embedded glove. The study compared glove-based control with computer vision-based control, analyzing their response speed, accuracy, cost, and efficiency for robotic hand teleoperation. The results demonstrated that the flex sensor-based glove provided more accurate and responsive control than the vision-based method, which was affected by lighting conditions and hand occlusion issues. However, the study did not present detailed quantitative performance evaluations. Additionally, the robotic hand was restricted to flexion and extension movements and lacked haptic feedback.

Li et al. [23] developed a marker-less vision-based hand-arm teleoperation system that integrates deep learning for hand pose estimation and an active vision system for improved tracking accuracy. To address occlusion issues, an active vision system dynamically adjusts the camera position for optimal hand observation. The system was tested on pick-and-place, pouring, stacking, and sweeping tasks, demonstrating good grasp stability and precise control. However, the approach has drawbacks, including high computational complexity, reliance on expensive depth cameras, and lack of direct haptic feedback. Xu et al. [24] developed a bimanual telerobotic system integrating bilateral haptic feedback, virtual reality (VR), and dexterous robotic hands to enhance immersion and precision in teleoperation. The system utilized exoskeleton gloves with force feedback motors and tactile sensors on the robotic hand's fingertips to provide real-time haptic interaction. Their experiments demonstrated that haptic feedback improved grasping precision, reduced cognitive load, and enhanced performance in blind grasping and fine manipulation tasks. However, the system had some drawbacks, including the complexity of VR-based control, reliance on expensive hardware like HTC Vive and ZED Mini, and limited sensitivity of tactile sensors in delicate grasping tasks.

Despite the extensive progress made by these authors, several critical gaps remain. Glove-based control approaches by Puruhita et al., Bhandari et al., and Al Qaradagi et al.,

as well as vision-based approaches by Coppola et al., and Li et al., suffer from the aforementioned drawbacks associated with control approaches, which reduce robustness and reliability in real-world settings. Virtual reality approaches by Zhang and Qian, and Xu et al. involve control complexity, rely on expensive hardware, and are limited to virtual object interaction, making them less applicable for real-world teleoperation. The robotic hands developed by Puruhita et al., Fu et al., and Al Qaradagi et al. lacked abduction and adduction capabilities, which are essential for efficiently grasping irregularly shaped objects. Furthermore, force sensing and feedback systems – crucial for precise control of applied force and for providing the user with a sense of presence at the remote site – were often absent in the works of Puruhita et al., Bhandari et al., Yamakawa et al., Fu et al., Al Qaradagi et al., and Li et al. These challenges highlight the need for a telerobotic hand that combines alternative control techniques with cost-effectiveness, dexterity, and intuitive force feedback.

To address these gaps, the present study developed and evaluated a low-cost, three-finger telerobotic hand for grasping small, multiform objects in remote locations while providing force feedback to the human operator at the local site. The system features an 11-DOF robotic hand with four distinct ranges of motion (ROMs) – abduction, adduction, flexion, and extension – controlled through a wireless platform that integrates a force feedback system into joysticks designed with adjustable positions to accommodate varying hand sizes. By combining enhanced motion capability with an affordable, user-friendly control interface, this work advances the deployment of telerobotic hands with potential for real-world applications in as agriculture, healthcare, space exploration, and disaster response.

2.0 MATERIALS AND METHODS

In this section, the system's description, architecture, working principle, design theories and methods are discussed.

2.1 Description of the System

The design of the robotic hand included incorporating four ROMs per hand digits for enhanced grasping capability. The tips of the robotic hand digits were equipped with force sensitive resistors (FSRs) to measure the pressure impressed by the grasped object on the digits. The design of the wireless controller platform involved the use of joysticks to control the robotic hand's digits. The joysticks were embedded with micro-vibration motors (MVMs) to provide the user with force feedback. Holes were made on the controller platform for two purposes: to allow for future expansion of the joysticks to control five digits of the robotic hand and to allow for adjustment of the joysticks to fit users with varying hand sizes. Figure 1 shows the 3D sketch of the three-finger robotic hand and the joystick-based controller.

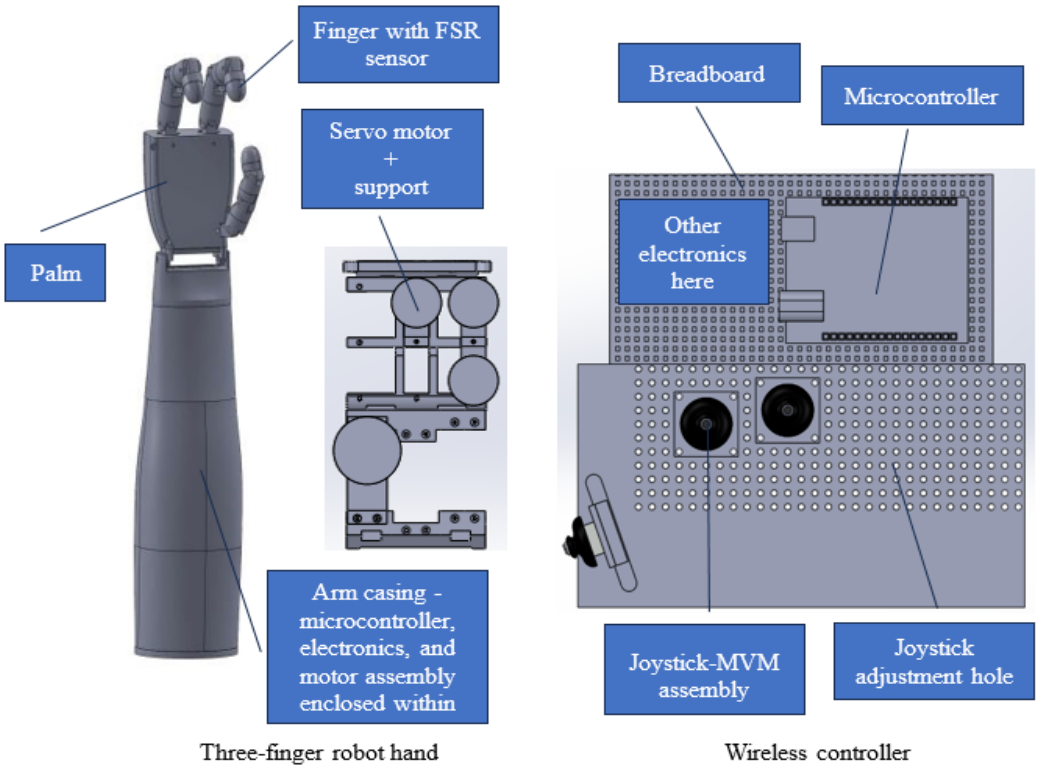

Figure 1: 3D sketch of the three-finger telerobotic hand

2.2 Architecture and Working Principle of the System

Table 1 presents the components used for developing the telerobotic hand, the function of each component, and the quantity required, while the block diagram of the telerobotic hand is presented in Fugure 2.

Table 1: List of components

S/N	Component	Function	Quantity
1.	Arduino Uno microcontroller	Interprets and processes signals, and control	2
2.	Joystick	Generates finger motion signals	3
3.	Servomotor Pulley Fishing line (beading thread)	Actuates the robot hand's digits Transmits power through rotation Serves as tendon to pull the digits	9 9
4.	FSR sensor	Measures fingertip force	3
5.	MVM	Produces vibration proportionate to force	3
6.	HC-05 Bluetooth module	Transmits and receives signals	2
7.	Breadboard	Assembly of components	2
8.	60 Watts (12V, 5A) adaptor 9 Watts (9V, 1A) adaptor XL4015 bulk converter	DC power source for the robotic hand DC power source for the controller DC-DC step down regulator for robot hand	1 1 2

9.	Resistor (3.3kΩ, 1kΩ)	Resist flow of current	3 each
	NPN transistor (BC337)	Amplifies voltage	3
	Zener diode (1N4001)	Maintains a constant output voltage	3
	Capacitor (1000μF)	Smooths out pulsating DC voltage	1
	Jumper cable	Connects components and electronics	
10.	Screw, and bolt and nut	Fastens parts together	

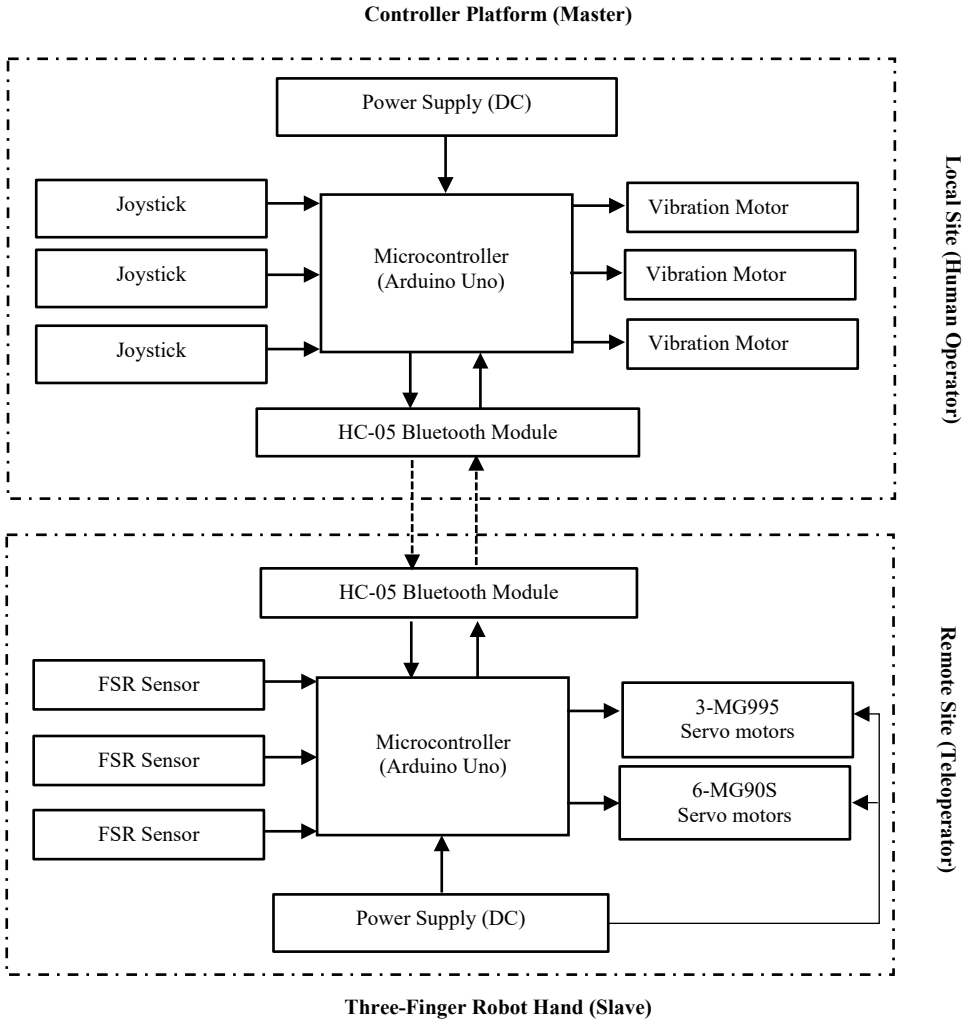

Figure 2: Block diagram of the telerobotic hand

The system operates as follows: The Arduino Uno microcontroller onboard the controller processes the joysticks' motion inputs from the operator's thumb, index, and middle fingers and transmits the control signals via the HC-05 Bluetooth module to the robotic hand. The Arduino Uno on the robotic hand receives these control signals through its HC-05 Bluetooth module and processes them to actuate the robot hand digits via tendons (fishing line) connected to the servo motors. When the robotic hand digits interact with an object, the Arduino Uno onboard the robotic hand processes the FSR sensors' signals and sends them through the HC-05 Bluetooth module to the controller. The controller receives these signals through its HC-05 Bluetooth module and processes them to drive the MVMs on the joysticks, with vibrations intensifying as the force exerted increases. The Arduino Uno microcontroller was selected for its low cost, wide library support, and provision of

sufficient computational capability for servo control, sensor acquisition, and Bluetooth communication. Figure 3 shows the flowchart of the telerobotic hand.

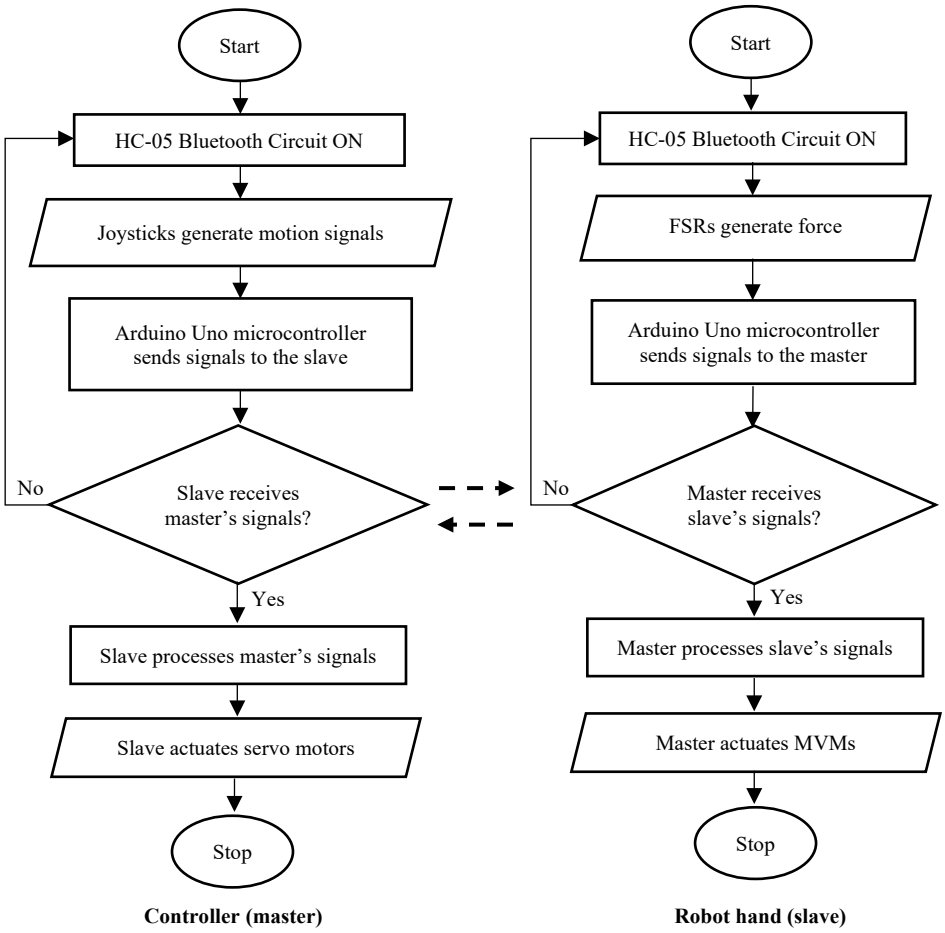

Figure 3: Flowchart of the telerobotic hand

2.3 Design Theory

2.3.1 Ranges of Motion

Ranges of Motion specifies the number of motions achievable by a robotic finger. In the human hand, ROMs include flexion, extension, abduction, adduction, opposition, and circumduction. In this work, circumduction (axial rotation of the digits) was constrained to reduce design and fabrication complexities. The ROMs of the Anatomically Correct Testbed (ACT) Hand for studying the intrinsic biomechanics and control of the human hand, developed by Deshpande et al. [25], were adopted – with slight modifications. The ACT Hand achieves close similarity in form and function to the human hand, with fingers actuated by anatomically routed tendons and both intrinsic and extrinsic muscle-equivalent actuators. Since the objective of this study was not to strictly replicate near-human hand motions ideal for object manipulation, certain constraints were applied: extension was limited to 0°, flexion was limited to 90° (except for the thumb's interphalangeal joint, which was set at 60° due to palm opposition), and abduction–adduction was limited to 30°. Table 2 presents the joint motion limits from [25], while Table 3 shows the modifications made in this study.

Table 2: Joint motion limits [25]

Finger	Joint	Minimum	Maximum
Index	MCP PIP DIP	30° extension, 35° abduction 0° extension 0° extension	90° flexion, 35° adduction 110° flexion 70° flexion
Middle	MCP PIP DIP	30° extension, 35° abduction 0° extension 0° extension	90° flexion, 35° adduction 110° flexion 70° flexion
Thumb	CMC MCP IP	40° extension, 40° abduction 60° extension, 15° abduction 20° extension	40° flexion, 40° adduction 60° flexion, 15° adduction 80° flexion

Table 3: Joint motion limits of the developed telerobotic hand

Finger	Joint	Minimum	Maximum
Index	MCP PIP DIP	0° extension, 30° abduction 0° extension 0° extension	90° flexion, 30° adduction 90° flexion 90° flexion
Middle	MCP PIP DIP	0° extension, 30° abduction 0° extension 0° extension	90° flexion, 30° adduction 90° flexion 90° flexion
Thumb	CMC MCP DIP	0° extension, 30° abduction 0° extension 0° extension	0° flexion, 30° adduction 60° flexion 90° flexion

2.3.2 Finger and Thumb Lengths

For tasks requiring a power grip, where the object is stabilized against the palm using full finger flexion, the fingers must wrap around a significant portion of the object's surface. In the case of cylindrical objects such as 35cl Coca-Cola plastic bottle used in this design, this is typically interpreted as wrapping around at least half of the object's circumference to ensure stable and secure contact. The circumference of the object of diameter D is given by the relation:

$$C = \pi D \quad \ldots 1$$

The total wrap reach required to enclose half the object is:

$$R = \frac{C}{2} \quad \ldots 2$$

Assuming that the robotic finger contributes about 95% of the wrap effort, the required finger length is:

$$L = 0.95R \quad \ldots 3$$

The total finger length is distributed across the proximal, middle, and distal phalanges. Table 4 shows human anatomical proportions extracted from [25]. By calculating the ratios r_3/r_1, r_2/r_1, and r_1/r_1 where r_1, r_2, and r_3 are the proportional lengths of the distal phalanx, medial phalanx, and proximal phalanx respectively, it is possible to estimate each digit's segment length based on the ratio r_1: r_2: r_3.

Table 4: Human hand anatomical proportions [25]

Finger	Proximal (mm)	Medial (mm)	Distal (mm)	Approximate (r_3: r_2: r_1)
Index	51.0	26.9	15.5	3.3:1.7:1
Middle	53.8	35.8	18.0	3.0:2.0:1
Thumb	43.1	36.5	20.0	2.2:1.8:1

The individual segment length l_{ij} is calculated as:

$$l_{ij} = L.\frac{r_i}{r_1 + r_2 + r_3} \quad \ldots 4$$

where the subscripts i and j represent the phalanx type and finger type respectively.
Finger length using a biomimetic optimization method based on the kinematic features of the *i*th human finger [26] are:

$$l_{1i} > l_{2i} > l_{3i} \quad \ldots 5$$

$$l_{1i} < (l_{2i} + l_{3i}) \quad \ldots 6$$

where l_{1i}, l_{2i}, and l_{3i} are the proximal, medial and distal lengths of the finger respectively.
The ratio of index finger length to thumb length [27] is given by:

$$\frac{l_{index}}{l_{thumb}} = 1.09 - 1.65 \quad \ldots 7$$

Table 5: Phalanx lengths of the developed telerobotic hand

Finger	Proximal phalanx (mm)	Medial phalanx (mm)	Distal phalanx (mm)
Index	40	25	19
Middle	40	25	19
Thumb	35	-	20

2.3.3 Radius of Flexion and Abduction Servomotor Pulley

By manually flexing the finger completely, it is possible to estimate the length of the tendon required to achieve full flex of the finger. The arc length (in radians) of the pulley corresponding to the tendon displacement [28] is given by:

$$\theta_1 = \frac{l_T}{r_{FP}} \quad \ldots 8$$

where: l_T is the tendon length required to cause full flexion of the finger, and r_{FP} is the flex pulley radius. From equation (8), the radius of the flexion pulley,

$$r_{FP} = \frac{l_T}{\theta_1} \quad \ldots 9$$

Similarly, the radius of the abduction pulley,

$$r_{AP} = \frac{l_A}{\theta_2} \quad \ldots 10$$

where: l_A is the tendon length required for full abduction.

2.3.4 Maximum Mass Lifting Capability of the Finger

Figures 4 shows a fully extended index finger with forces F_1 and F_2 acting on it. Doğan [29] established equations (11) – (12) for calculating F_1 and F_2. Equation (13) converts force to gram, while equation (14) sums the mass lifting capability of the three hand digits.

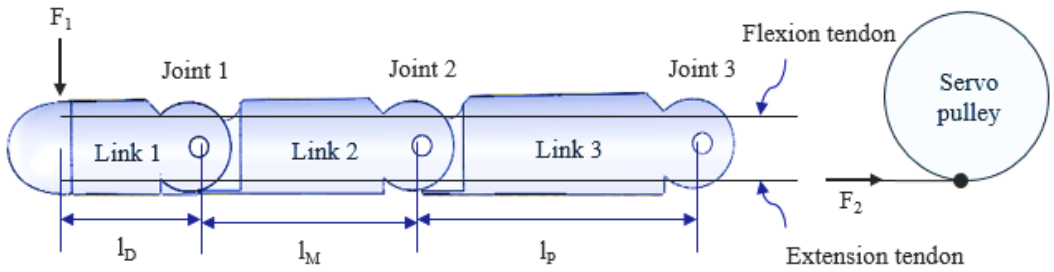

Figure 4: Forces acting on index finger of the developed robotic hand

F_1 is the force applied near the tip of the finger and F_2 is the tension in the tendon. Moment is created by the tendons about each joint in the finger. The moment created at joint 3 is the greatest since it is the furthest away from F_1. The turning force at joint 3 limits the load that can be lifted at the tip of the finger. The moment, M_1 equals M_2 at the point where the maximum load can be lifted.

$$F_1(l_P + l_M + l_D) = F_2 R_{J3} \quad \ldots\ldots 11$$

where: l_P, l_M, and l_D are the proximal length, medial length, and distal length respectively, and R_{J3} is the radius of pulley at joint 3.

For the finger to flex completely with the attached load, the diameter of the pulley in Figure 4, given by $d_P = 2.r_{FP}$ must be large enough to cause full displacement of the tendon.

$$F_2 = \frac{\tau_S}{d_P} \quad \ldots\ldots 12$$

where τ_S is the stall torque of the servo motor, Nm.

Mass lifting capability of the index finger:

$$m_{index} = 101.97 \times F_1 \quad \ldots\ldots 13$$

Total maximum mass lifting capability,

$$m_{max} = m_{index} + m_{middle} + m_{thumb} \quad \ldots\ldots 14$$

2.3.5 Minimum Gripping Force

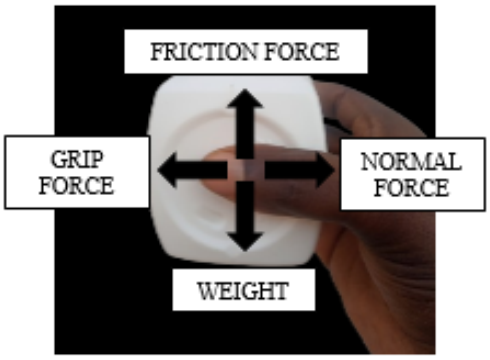

Figure 5: FBD of static forces on an object

Gripping force is needed to calculate the power input required by the gripper mechanism so that it can grasp and retain an object. Equations (15) – (20) are extracted from Lai [30]. Figure 5 shows the free body diagram (FBD) of static forces acting on an object.

The static friction force must be equal to the weight of the object to maintain the object from slipping out of the robot hand.
Force in the vertical direction:

$$\sum F_y = F_f - W = 0 \quad \ldots\ldots 15$$

where: F_f is the frictional force, and W is the weight of the object.
Force in the horizontal direction:

$$\sum F_x = F_g - N = 0 \quad \ldots\ldots 16$$

where: F_g is the gripping force, and N is the normal force.
The frictional force, F_f is given by

$$F_f = \mu N \quad \ldots\ldots 17$$

where: μ is the coefficient of static friction and N, the normal force, is equal in magnitude but opposite to the gripping force.
Substituting equation 17 in equation 15

$$\mu N = W \quad \ldots\ldots 18$$

where the weight of the object, W is:

$$W = m(g + a) \quad \ldots\ldots 19$$

where: m is maximum mass that the robotic hand can lift, g is gravitational force, and a is acceleration of the robotic hand taken as zero to avoid adding weight to the plastic bottle.
From equations 16 and 18, the gripping force produced by the three fingers is:

$$F_g = \frac{W}{3\mu}.S \quad \ldots\ldots 20$$

where: S is the safety factor.

2.3.6 Robot Hand and Controller Power Requirements

The main component in the robot hand that consumes power is the servo motor. The servo motors are powered with a separate 6V stepped down from a 60 Watts (12V, 5A) adaptor. The power consumed by servo motor [31],

$$P_S = I_T \times V \quad \ldots\ldots 21$$

where: I_T is the total current drawn by the servos, and V is the voltage.
Current drawn by n servos,

$$I = nI_S \quad \ldots\ldots 22$$

where: n is the number of servos, and I_S is the stall current of the servo at the operating voltage.
Depending on the usage, the servos won't be at stall torque all the time. Assuming 25% duty cycle (active movement vs. idle), total current drawn by servos [32],

$$I_T = \frac{25}{100} \times I \quad \ldots\ldots 23$$

Power requirement for other electronic components except XL4015 DC-DC buck converter can be estimated using [31]:

$$P_i = I_C \times V_C \quad \ldots\ldots 24$$

where: I_C is the current drawn by the component, V_C is the operating voltage of the component, and i represents the component name.
Power requirement for XL4015 DC-DC buck converter depends on power delivered to load, efficiency of XL4015, and power drawn from the source [33].
Power delivered to load is given by [31]:

$$P_{out} = V_{out} \times I_{out} \quad \ldots\ldots 25$$

The efficiency of XL4015 is up to 96%. Assuming an efficiency of 90%, power drawn from the source [31]:

$$P_{in} = \frac{P_{out}}{\eta} \quad \ldots 26$$

2.4 Assembly of the Robot Hand and the Wireless Controller

Figure 6 shows the developed telerobotic hand. The circuit diagram of the robotic hand and wireless controller are presented in Figure 7 and Figure 8 respectively.

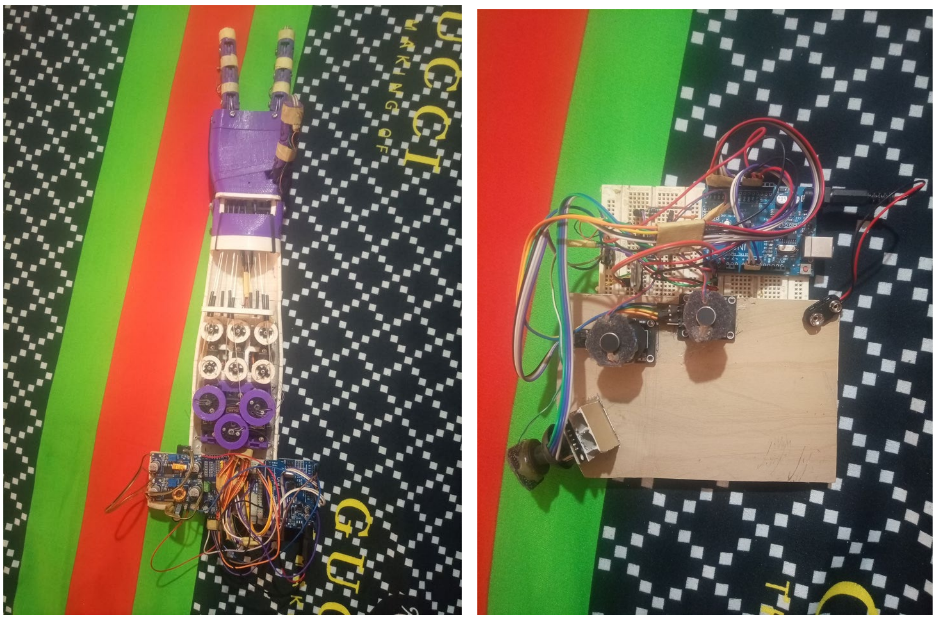

Robotic hand | Controller

Figure 6: The developed telerobotic hand

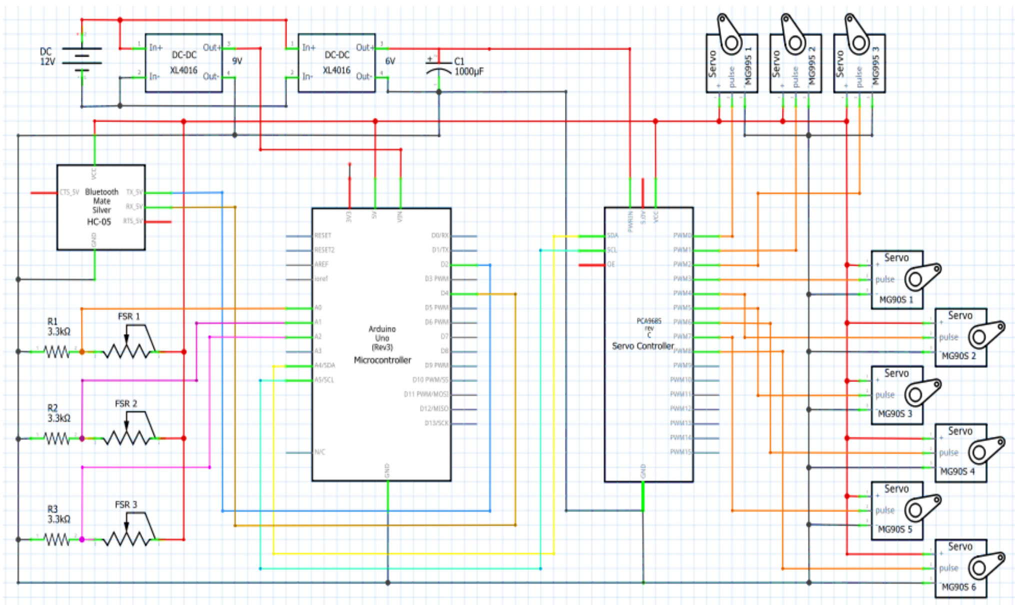

Figure 7: Robot hand circuit diagram

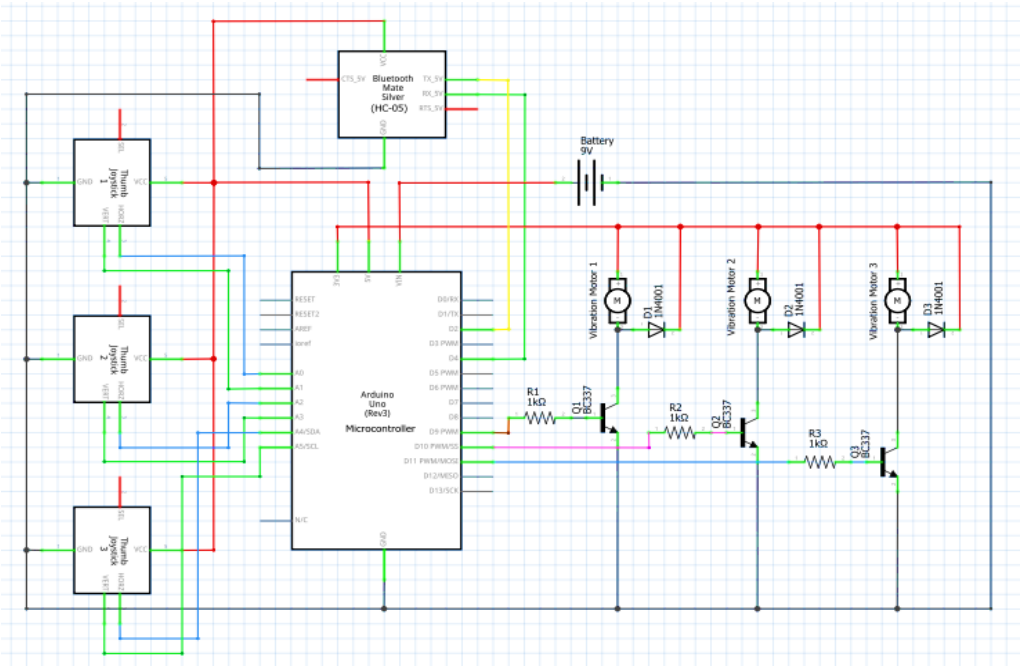

Figure 8: Controller circuit diagram

3.0 EVALUATION OF THE TELEROBOTIC HAND

The performance evaluation of the telerobotic hand was categorized into five distinct assessment domains:

3.1 Motion Accuracy Test

Motion accuracy test was conducted to evaluate how accurately and consistently the robotic fingers replicated the motions initiatiated by the joysticks. The joysticks were then manually tilted to predefined directions corresponding to specific servo commands. The desired servo angles were the servomotors angles required to make the robotic hand digits flex/extend or abduct/adduct while the actual angles were the angles achieved by the servomotors when controlled by the joysticks. The actual servo angle achieved by the robotic hand was monitored and recorded in real-time via the Arduino IDE serial monitor. For motion repeatability, the motion accuracy test was repeated five times. The mean, absolute error, percentage error, and standard deviation were then computed. The results were plotted using bar charts with error bars to represent the standard deviation and reliability of the servo response at each input level, and line graphs to track angular trends across repetitions.

3.2 Grasping Efficiency Test

Grasping efficiency of the robotic hand was evaluated by assessing its ability to grasp and securely hold a range of household objects with varying shapes, sizes, and surface. The household objects included soap-box, cello tape, spray-can, cream-box, extension socket, and hairbrush as experimented in Figure 9.

Figure 9: Multiform objects selected and grasped by the telerobotic system

During the test, the operator manipulated the robotic fingers via the wireless controller in an attempt to grasp the household objects of interest shown in Figure 9. A grasp was considered successful if the object remained stable in the robotic hand for at least five seconds without slipping or dropping. The test was repeated five times, and the number of successful grasps was recorded. The grasping efficiency for each object was obtained using equation (27):

$$Grasping\ Efficiency\ (\%) = \frac{\sum Successful\ Grasps}{\sum Total\ Grasp\ Attempts} \times 100 \ldots\ldots\ldots\ldots\ldots\ldots\ldots 27$$

The overall grasping performance of the robotic hand was analyzed using: bar charts to display success rates for individual objects, and pie charts to show the proportion of successful versus failed grasps.

3.3 Object Grasping Time-taken Test

Object grasping time-taken test was carried out to evaluate the responsiveness of the telerobotic hand in real-time object grasping using the six household objects of interest.

Figure 9: Multiform objects selected and grasped by the telerobotic system

Grasp command was initiated using the wireless controller and the time taken from the moment the command was given until the object was securely grasped was recorded with the aid of a digital stopwatch. For each object, the test was repeated five times under the same conditions to ensure consistency. The average time for each object was calculated, followed by the computation of the overall average grasping time using equation (28):

$$Overall\ Average\ Time = \frac{\sum Average\ Time\ for\ Each\ Object}{Number\ of\ Objects} \quad \ldots\ldots\ldots\ldots\ldots\ldots\ldots 28$$

The result was analyzed using bar charts to compare the average grasping times across different objects. Bar charts with error bars were used to analyse variability in grasping across trials.

3.4 Force Sensitivity and Haptic Feedback Test

Force sensitivity and haptic feedback test was conducted to assess the ability of the telerobotic hand to detect varying gripping forces through FSR sensors and to transmit corresponding real-time feedback via MVMs on the joystick-based wireless controller. Each household object of interest was grasped with the robotic hand while the FSR sensors embedded on the fingertips of the robotic fingers captured the gripping force applied during each trial and the MVMs on the joystick vibrate with intensity proportional to the applied force.

For each object, the test was repeated five times to ensure consistency. The average force readings from the force-sensitive resistor sensors and the corresponding vibration intensity levels of the micro-vibration motors displayed on the Arduino IDE serial monitor were recorded. The data collected were analyzed to determine the correlation between the force sensing and the force feedback. The results were visualized using bar charts to illustrate variations in force levels and corresponding feedback intensity across different fingers and objects.

3.5 User Experience and Ergonomics Test

User experience and ergonomics test was conducted to assess the comfort, ease of use, responsiveness, haptic feedback, fatigue level, and grasp completion of the robotic hand's control interface during grasping operations.

Five participants having varying hand size and with no prior experience using the system were selected for the test. Each participant was given a brief training session to understand the joystick control scheme and the purpose of the experiment. During the test, participants were instructed to grasp each of the household objects of interest with the robot hand and give their observations and ratings across six metrics based on the Likert scale presented in Table 6. The user ratings were analyzed using bar charts to compare individual feedback.

Table 6: Likert ratings for user experience and ergonomics test

Test	Ratings				
	1	**2**	**3**	**4**	**5**
Comfort	Very uncomfortable	Uncomfortable	Neutral	Comfortable	Very comfortable
Ease of use	Very difficult	Difficult	Neutral	Easy	Very easy
Responsiveness	Very poor	Poor	Moderate	Good	Excellent
Haptics	Very poor	Poor	Moderate	Good	Excellent
Fatigue level	Very fatigued	Fatigued	Moderate	Minimal	No fatigue
Grasps	Very slow	Slow	Moderate	Fast	Very fast

4.0 RESULTS AND DISCUSSION

The development and evaluation of the telerobotic hand with force feedback revealed multiple important findings regarding motion accuracy, grasping efficiency, grasping time-taken, haptic responsiveness, and user factors. This section interprets these results, explains their underlying mechanisms, situates them within existing teleoperation literature, and highlights their broader technological and application implications.

4.1 Motion Accuracy

Figure 10 illustrates the robot hand's digits motion replication of the wireless controller's motion inputs across five trials, while Figure 11 illustrates motion accuracy of the robot hand's digits with deviations.

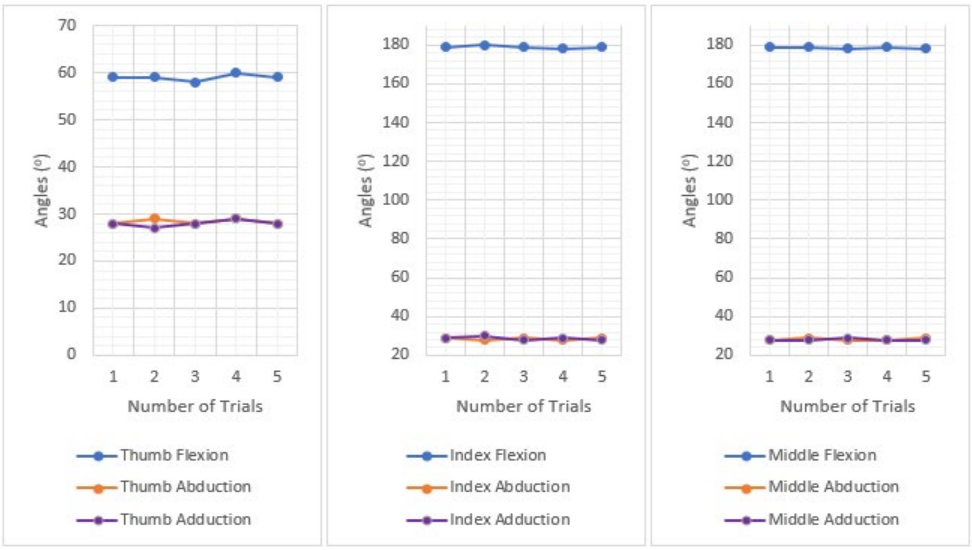

Figure 10: Robot hand's digits motion replication across five trials

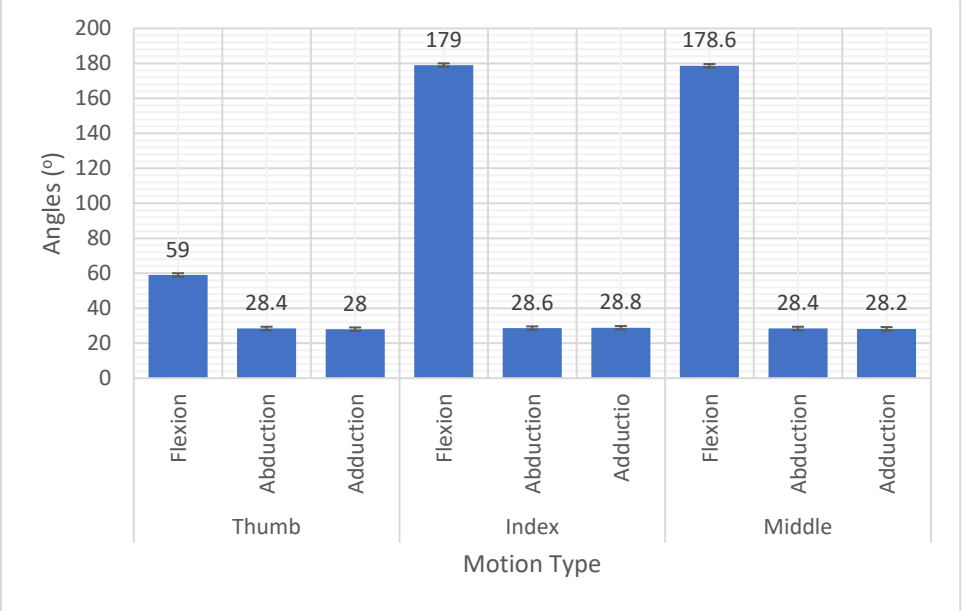

Figure 11: Robot hand's digit motion accuracy with deviations

For full flexion of the thumb, index finger, and middle finger, the desired servomotor angles were 60°, 180°, and 180°, respectively. For full abduction/adduction, the desired angles for the three digits were 30°, 30°, and 30°, respectively. The points in Figure 10 represent the actual servomotor angles over five trials. The proximity of these points to the desired angles indicates that the robotic hand followed joystick inputs with high fidelity.

Figure 11 shows that the thumb recorded an average error of 1° (1.6%) in flexion, 1.6° (5.3%) in abduction, and 2° (6.6%) in adduction. The index finger showed an error of 1° (0.5%) in flexion, with errors of 1.4° (4.6%) and 1.2° (4.0%) in abduction and adduction, respectively. The middle finger exhibited an error of 1.4° (0.7%) in flexion, 1.6° (5.3%) in abduction, and 1.8° (6.0%) in adduction. Figure 11 also shows that the thumb had a minimal standard deviation of 0.71° in flexion, 0.55° in abduction, and 0.71° in adduction. For the index finger, deviations were 0.71° in flexion, 0.55° in abduction, and 0.84° in adduction. The middle finger recorded deviations of 0.55° in flexion, 0.55° in abduction, and 0.45° in adduction. These low standard deviation values across all digits confirm that the robotic hand executed repeated motions with high accuracy and predictability.

The overall motion accuracy of 96.2%, comprising 99.1% for flexion and 94.75% for abduction/adduction, demonstrates the effectiveness of the tendon-driven actuation system while also revealing design-dependent limitations. The superior accuracy in flexion can be attributed to the mechanical simplicity of tendon routing, where tendons aligned with the finger's longitudinal axis experience lower friction and minimal slippage. By contrast, the slightly reduced accuracy in lateral motions was likely due to mechanical tolerances arising from plastic–plastic contact at the revolute joints and backlash in tendon routing for abduction/adduction, which introduce additional friction points and angular misalignments. This disparity resulted in a 5.25% reduction in lateral accuracy, suggesting potential improvements such as tighter CAD model tolerances, integration of micro-ball bearings, or the use of tendon-routing tubes to reduce friction.

Comparable glove-based systems have achieved finger tracking errors of about 2.83% [16] or 98.6% accuracy [19], while vision-based approaches have reached 96.5% accuracy [19] but at significantly higher computational cost. In contrast, the present joystick-driven design achieved near-equivalent performance without calibration drift or sensitivity to lighting conditions, which often hinder glove-based and vision-based systems

[14, 15]. From a control perspective, this level of accuracy is sufficient for tasks requiring simple flexion and extension, such as warehouse pick-and-place operations. However, for more demanding applications, such as surgical manipulation or satellite servicing, the reduced lateral precision may require operator compensation strategies or improved actuation mechanisms.

4.2 Grasping Efficiency

Figure 12 shows the robotic hand's grasping success/failure rate and efficiency distribution.

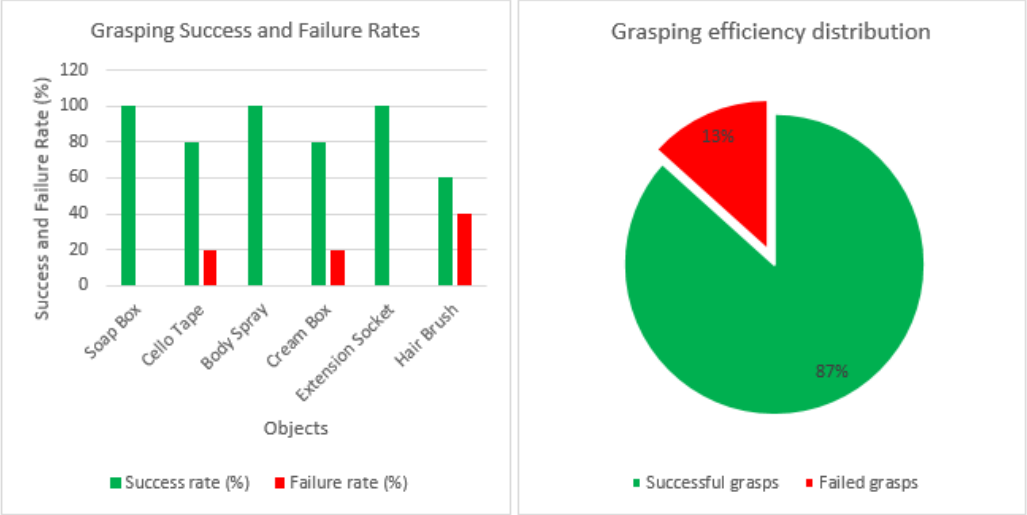

Figure 12: Grasping success and failure rates and efficiency distribution

The grasping efficiency test showed an overall success rate of 87%, highlighting both the strengths and limitations of the three-finger configuration. Rectangular objects (soap-box and extension socket) and cylindrical objects (spray-can) achieved 100% success due to geometric compatibility, as finger spacing and closure trajectories naturally aligned with predictable contact surfaces. Conversely, irregular objects such as the hairbrush were grasped with only 60% success, primarily due to uneven weight distribution and bristled contact surfaces, which disrupted force closure and reduced stability.

Although earlier studies did not quantify grasping efficiency in the same manner, the present findings mirror the trends reported by Coppola et al. [20], who observed improved grasping success when vibrotactile feedback was introduced, but whose Leap Motion sensor suffered from tracking inconsistencies with irregular objects. Similarly, Al Qaradagi et al. [22] demonstrated effective control using flex-sensor gloves; however, the absence of abduction/adduction motions limited their system's ability to handle multiform geometries. By contrast, the inclusion of abduction–adduction in the present work addresses this critical limitation, thereby improving versatility in irregular object manipulation.

The predictable performance observed with geometric objects indicates that the system is well-suited for industrial applications such as warehouse automation and assembly tasks. However, the reduced performance with irregular geometries may restrict deployment in medical applications, where delicate and complex-shaped instruments must be handled reliably, or in search-and-rescue operations, where objects are often unstructured and unpredictable.

4.3 Object Grasping Time-taken

Figure 13 presents the results of the average time taken by the robotic hand to grasp each object over five trials. The findings show that the grasping time varied depending on the object's shape, size, and surface texture. Rectangular objects such as soap-boxes were grasped fastest (1.6 s) due to stable surface interactions and predictable geometry. In contrast, irregular objects such as the hairbrush required the longest time (2.6 s), likely due to its asymmetric shape and bristles, which made it more challenging for the robotic fingers to establish a secure grip.

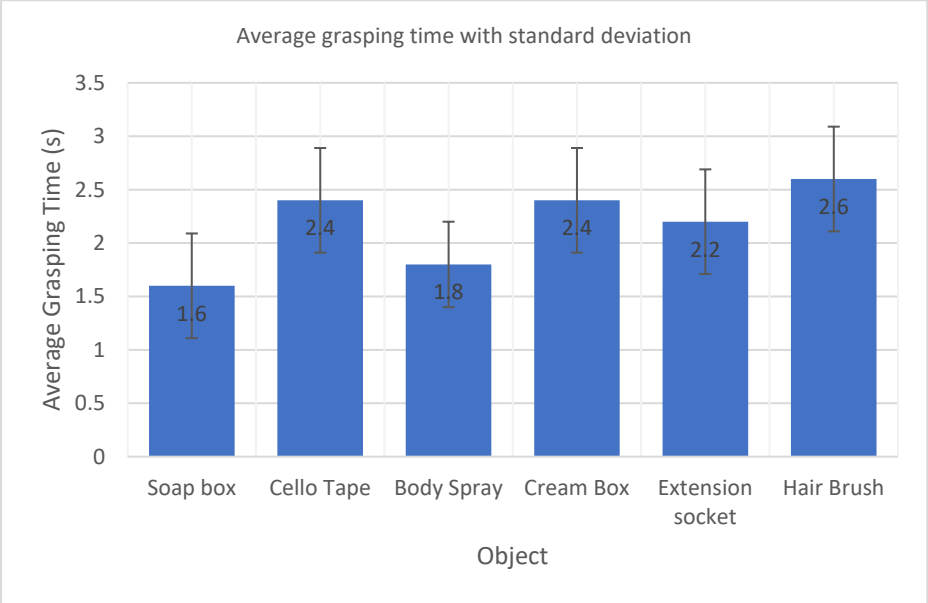

Figure 13: Average grasping time with standard deviation

Although slower than the ultra-low latency (< 20 ms) reported by Yamakawa et al. [18] using high-speed vision-based sensing, the present system achieved adequate grasping times without relying on costly imaging hardware. This balance between performance and affordability highlights the practicality of the joystick-driven approach, particularly for applications in low- and middle-income contexts where resource constraints may preclude high-end sensing systems.

The variability in grasping time was analyzed using the standard deviation. The spray-can exhibited the lowest variability with standard deviation of 0.40, indicating that it was grasped with consistent speed across trials. By contrast, the soap-box, cello-tape, cream-box, extension-socket, and hairbrush all recorded a standard deviation of 0.49, suggesting slightly higher but comparable variation. This consistency across most objects confirms the reliability of the system, although irregular geometries clearly posed greater challenges.

These results suggest that the robotic hand is highly effective for objects with simple, predictable geometries, making it suitable for industrial applications such as warehouse automation and structured assembly tasks.

4.4 Force Sensitivity and Haptics (Force) Feedback

Figure 14 represents the average measured force versus vibration intensity across the robotic hand digits recorded over five trials by the FSRs. The findings indicated that

increased applied force generally led to stronger haptic feedback, confirming that force-sensitive feedback mechanisms effectively captured variations in grip and material properties. The slight variations in force across fingers and trials highlighted differences in grip consistency and pressure distribution among fingers.

The measured force versus vibration intensity chart demonstrated a positive correlation between applied force and vibration intensity. Objects with lower forces (e.g. cello-tape, 3.00 – 3.16N) exhibited weaker vibrations (81 – 85PWM), indicating relatively unsatisfactory operator awareness. The spray-can, cream-box, and hairbrush showed moderate force levels, with slight variations between fingers and trials. Objects with higher measured forces (e.g. extension socket, 7.80 – 7.84N) resulted in stronger haptic feedback (212 – 215PWM), indicating fine operator awareness of grasp stability. This confirms findings by Xu et al. [24], who observed that haptic cues reduce cognitive load and improve task performance in teleoperation.

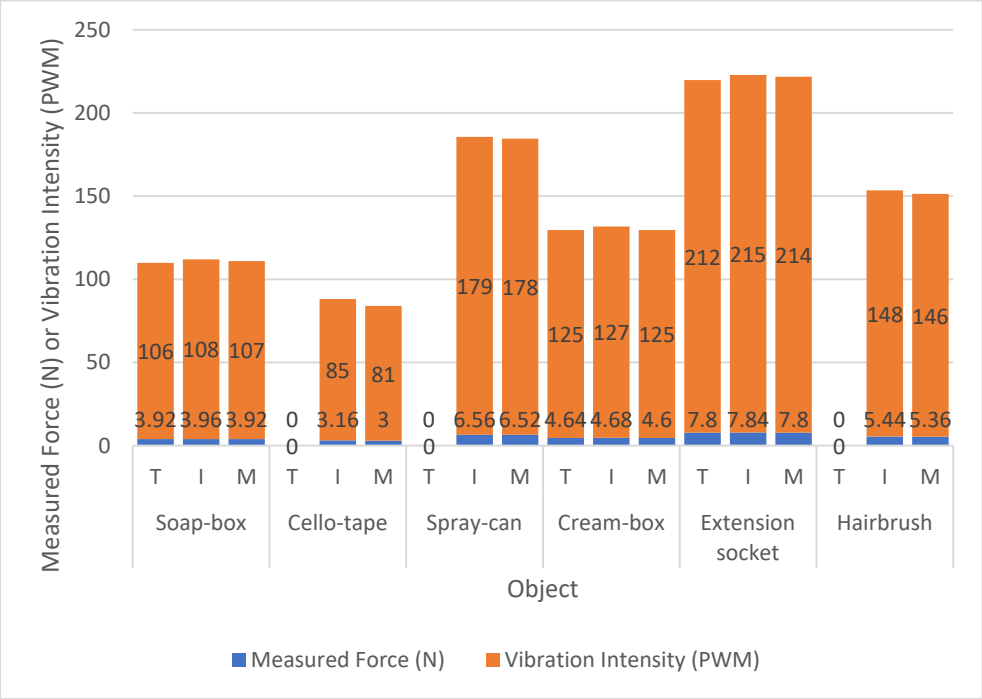

Figure 14: Measured force versus vibration intensity across the robotic hand digits

Despite the proportional correlation between fingertip forces and vibration intensity, the reliability of the present FSR configuration is a concern. Occasional zero readings, particularly at the thumb, reveal limitations in sensor placement and surface conformity. Unlike human tactile sensing, which dynamically adapts to objects, rigid FSR mounting restricts feedback consistency. Such inconsistencies in human–robot interaction may erode operator trust [13].

This underscores a trade-off between affordability and reliability. While high-end systems integrate tactile arrays, the present work demonstrates that even simple feedback mechanisms can provide meaningful utility – but with clear constraints for high-risk environments such as telemedicine or nuclear decommissioning.

4.5 User Experience and Ergonomics

Figure 15 shows the satisfaction level of five users across the household objects of interest. User studies revealed that the telerobotic hand achieved an average of 84% user satisfaction ratings across all metrics.

Figure 15: User experience and ergonomics satisfaction ratings

Responsiveness averaged 4.8 out of 5 (96%) satisfaction rate, and ease of use, 4.6 out of 5 (92%) satisfaction rate, validating the intuitiveness of joystick-based teleoperation. Comfort, haptic feedback, and task completion all averaged 4.2 out of 5 (84%) satisfaction rate. Nonetheless, fatigue ratings (64%) reveal ergonomic limitations inherent to sustained joystick use, indicating that while most users found the device comfortable and easy to use, fatigue remains an area requiring further investigation and potential ergonomic adjustments, possibly redesign of the wireless controller platform, to enhance user experience.

An overall 84% satisfaction rating suggests that the system is both intuitive and acceptable for short-term tasks which makes it promising for applications such as industrial pick-and-place operations where operation times are limited. However, the lower fatigue rating highlights a potential barrier to adoption in scenarios requiring extended use, such as healthcare procedures, or emergency response where user comfort and endurance are critical to sustained performance.

5.0 CONCLUSION

This research successfully developed and evaluated a low-cost prototype of a three-finger robotic hand capable of grasping multiform objects, controlled via a joystick-based wireless controller. The system achieved an overall motion accuracy of 96.2%, comprising 99.1% for flexion and 94.75% for abduction/adduction, confirming the effectiveness of the tendon-driven actuation system in reliably replicating teleoperated motions. However, the slight 5.25% reduction in lateral motions – likely due to mechanical tolerances and backlash in tendon routing for abduction/adduction – suggests potential improvements such as

tighter CAD model tolerances, integration of micro-ball bearings, optimized tendon–pulley geometries, or hybrid tendon–gear systems.

The system achieved a grasping efficiency of 87%, demonstrating effectiveness for structured tasks with rectangular or cylindrical geometries where finger spacing and closure trajectories naturally aligned with predictable contact surfaces. However, performance was less reliable for irregular objects with uneven weight distribution and deformable contact surfaces, such as the hairbrush, which disrupted force closure and reduced stability. This suggests that future work should focus on adaptive grasping strategies or expanding from a three-finger to a five-finger configuration with a foldable palm, thereby enhancing versatility and improving force closure on complex geometries.

Average grasping times ranged from 1.6 s for regular objects to 2.6 s for irregular objects, demonstrating adequate responsiveness and a balance between performance and affordability, highlighting the practicality of the joystick-driven approach without reliance on costly vision-based hardware. This makes the system particularly suitable for applications in low- and middle-income contexts where resource constraints may preclude high-end sensing systems. However, slower grasping times with irregular objects indicate the need for mechanical refinements and control strategies to reduce delays and improve versatility.

The evaluation of the force feedback mechanism indicated that increased applied force generally led to stronger haptic feedback, confirming that force-sensitive feedback mechanisms effectively captured variations in grip and material properties. The proportional correlation between measured force and vibration intensity implies that haptic feedback can enhance operator awareness of grasp stability. However, inconsistent sensor readings – particularly when fingertips had no direct contact with the object – limit reliability and may reduce user trust in critical applications. Future work should therefore explore distributed tactile sensors, improved sensor placement, and advanced haptic feedback strategies to ensure consistent, reliable performance across diverse object geometries.

User studies showed an average satisfaction rating of 84% for overall user experience and ergonomics. This indicates that while the system is intuitive and suitable for short-duration tasks, its limited fatigue performance may hinder acceptance in long, continuous operations where comfort and endurance are essential. Future work should focus on the ergonomic redesign of the control platform to minimize strain during prolonged use.

Based on the system's performance and potential use cases, the following quantifiable and targeted recommendations are proposed:

1. To enhance hand configuration, a robotic hand with a foldable palm and a five-finger configuration, with each finger featuring at least four ranges of motion should be developed to improve object grasping and manipulation versatility, potentially increasing the grasp success rate by 10–15%, especially for irregularly shaped objects.
2. For operation in extreme environments (e.g., underwater, space, or high-temperature zones), the robotic hand should be redesigned using engineering-grade materials such as polyoxymethylene (POM), carbon-fiber-reinforced nylon, aluminum alloy, or lightweight steel, which offer temperature resistance above 150 °C. In addition, micro-ball bearings should be incorporated at all digit joints to reduce frictional losses, improve response time, and enable axial finger rotation.
3. For more natural and intuitive gesture interpretation with increased tracking accuracy, a fingertip-wearable wireless controller incorporating a 6-DOF inertial measurement unit (IMU) should be developed and complemented with hardware and software filtering algorithms (e.g., Kalman filter or complementary filter) to enhance signal stability and tracking precision.

ACKNOWLEDGEMENT

The authors would like to express their sincere gratitude to Ahmadu Bello University, Zaria, and the National Space Research and Development Agency, Abuja, for providing the resources and facilities necessary for the completion of this research. We also extend our appreciation to colleagues whose support and contributions have greatly aided this work on various occasions.

CONFLICT OF INTEREST

The authors declare that there is no conflict of interest regarding the publication of this paper.

REFERENCES

[1] Niemeyer, G., Preusche, C., & Hirzinger, G. (2008). Telerobotics. In B. Siciliano & O. Khatib (Eds.), *Springer handbook of robotics* (pp. 741–757). Springer-Verlag.

[2] Yamakawa, Y., Katsuki, Y., Watanabe, Y., & Ishikawa, M. (2021). Development of a high-speed, low-latency telemanipulated robot hand system. *Robotics, 10*(1), 1–21. https://doi.org/10.3390/robotics10010041

[3] Li, S., Jiang, J., Ruppel, P., Liang, H., Ma, X., Hendrich, N., . . . Zhang, J. (2020). A mobile robot hand-arm teleoperation system by vision and IMU. In *2020 IEEE/RSJ International Conference on Intelligent Robots and Systems (IROS)* (pp. 10900–10906). IEEE.

[4] Zhang, Z., & Qian, C. (2023). Wearable teleoperation controller with 2-DoF robotic arm and haptic feedback for enhanced interaction in virtual reality. *Frontiers in Neurorobotics, 17*, 1–20. https://doi.org/10.3389/fnbot.2023.1228587

[5] Li, Z., Moran, P., Dong, Q., Shaw, R. J., & Hauser, K. (2017). Development of a tele-nursing mobile manipulator for remote care-giving in quarantine areas. In *2017 IEEE International Conference on Robotics and Automation (ICRA)* (pp. 3581–3586). IEEE.

[6] Nagatani, K., Kiribayashi, S., Okada, Y., Otake, K., Yoshida, K., Tadokoro, S., . . . Kawatsuma, S. (2013). Emergency response to the nuclear accident at the Fukushima Daiichi Nuclear Power Plants using mobile rescue robots. *Journal of Field Robotics, 30*(1), 44–63.

[7] NASA. (2021). *Robonaut program overview*. NASA. Retrieved September 1, 2025, from https://www.nasa.gov/robonaut

[8] Fortune Business Insights. (2020). *Telerobotics market size, share & COVID-19 impact analysis, by component, by application, and regional forecast, 2020–2027*. Fortune Business Insights. Retrieved September 1, 2025, from https://www.fortunebusinessinsights.com

[9] Amaifeobu, O., Iyamu, O., & Adewunmi, A. (2023). Opportunities and barriers for adopting robotics in Nigerian construction industry. *International Journal of Research Publication and Reviews, 4*(1), 535–543.

[10] Burke, J., Gnanaraj, J., Dhanda, J., Martins, B., Vinck, E. E., Saklani, A., & Harji, D. (2024). Robotic surgery in low- and middle-income countries. *The Bulletin of the Royal College of Surgeons of England, 106*(3), 138–141.

[11] Becher, B. (2024). *What are robotic hands? What can they do?* Built In. Retrieved September 1, 2025, from https://builtin.com/articles/robotic-hand

[12] Ma, R. R., & Dollar, A. M. (2011). On dexterity and dexterous manipulation. In *2011 15th International Conference on Advanced Robotics (ICAR)* (pp. 1–7). IEEE.

[13] Ang, B. W., Yeow, C. H., & Lim, J. H. (2023). A critical review on factors affecting the user adoption of wearable and soft robotics. *Sensors, 23*(6), 1–22.

[14] Alkkiomäki, O., Kyrki, V., Kälviäinen, H., Liu, Y., & Handroos, H. (2008). Challenges of vision for real-time sensor-based control. In *2008 Canadian Conference on Computer and Robot Vision* (pp. 42–49). IEEE.

[15] Shahria, M. T., Sunny, M. S., Zarif, M. I., Ghommam, J., Ahamed, S. I., & Rahman, M. H. (2022). A comprehensive review of vision-based robotic applications: Current state, components, approaches, barriers, and potential solutions. *Robotics, 11*(6), 139. https://doi.org/10.3390/robotics11060139

[16] Puruhita, S., Satria, N., Hanafi, N., & Kusumawati, E. (2020). Development of teleoperation humanoid robot hand mimicking through human hand movement. In *2020 International Electronics Symposium (IES)* (pp. 277–283). IEEE.

[17] Bhandari, S., Bindal, R., Sharma, P., Zubair, M., & Jain, D. (2021). Design of robotic hand and wireless glove to tele-operate. In *Proceedings of the 2021 5th International Conference on Advances in Robotics* (pp. 1–5). ACM.
[18] Yamakawa, Y., Katsuki, Y., Watanabe, Y., & Ishikawa, M. (2021). Development of a high-speed, low-latency telemanipulated robot hand system. *Robotics, 10*(1), 1–21. https://doi.org/10.3390/robotics10010041
[19] Fu, J., Poletti, M., Liu, Q., Iovene, E., Su, H., Ferrigno, G., & De Momi, E. (2022). Teleoperation control of an underactuated bionic hand: Comparison between wearable and vision-tracking-based methods. *Robotics, 11*(3). https://doi.org/10.3390/robotics11030061
[20] Coppola, C., Solak, G., & Jamone, L. (2022). An affordable system for the teleoperation of dexterous robotic hands using leap motion hand tracking and vibrotactile feedback. In *2022 31st IEEE International Conference on Robot and Human Interactive Communication (RO-MAN)* (pp. 920–926). IEEE.
[21] Zhang, Z., & Qian, C. (2023). Wearable teleoperation controller with 2-DoF robotic arm and haptic feedback for enhanced interaction in virtual reality. *Frontiers in Neurorobotics, 17*, 1–20. https://doi.org/10.3389/fnbot.2023.1228587
[22] Al Qaradagi, M., Ameen, F., Benotsmane, R., & Miatliuk, K. (2024). Application of teleoperation control for a robotic hand using a glove. In *2024 25th International Carpathian Control Conference (ICCC)* (pp. 1–6). IEEE.
[23] Li, S., Hendrich, N., Liang, H., Ruppel, P., Zhang, C., & Zhang, J. (2024). A dexterous hand-arm teleoperation system based on hand pose estimation and active vision. *IEEE Transactions on Cybernetics, 54*(3), 1417–1428.
[24] Xu, H., Chen, M., Li, G., Wei, L., Peng, S., Xu, H., & Li, Q. (2025). An immersive virtual reality bimanual telerobotic system with haptic feedback. *arXiv preprint*, arXiv:2501.00822.
[25] Deshpande, A. D., Xu, Z., Vande Weghe, M. J., Brown, B. H., Ko, J., Chang, L. Y., & Matsuoka, Y. (2013). Mechanisms of the anatomically correct testbed hand. *IEEE/ASME Transactions on Mechatronics, 18*(1), 238–250.
[26] Kim, B. H. (2015). Effective length design of humanoid robot fingers using biomimetic optimization. *International Journal of Advanced Robotic Systems, 12*(10), 150.
[27] Chen, X., Li, Z., Wang, Y., Liu, J., & Zhao, D. (2019). Investigation on the cooperative grasping capabilities of human thumb and index finger. *Frontiers in Neurorobotics, 13*, 92.
[28] Study.com. (2021). *How to find arc length in radians | Geometry*. Retrieved September 4, 2025, from https://study.com/skill/learn/how-to-find-arc-length-in-radians-explanation.html
[29] Doğan, B. (2010). *Development of a two-fingered and a four-fingered robotic gripper* (Master's thesis). Middle East Technical University.
[30] Lai, M. (2016). *Fall 2016 prosthetic hand: Force and torque calculation*. Arxterra. Retrieved September 1, 2025. https://www.arxterra.com/fall-2016-prosthetic-hand-force-and-torque-calculations/
[31] Erickson, R. W. (2000). *Fundamentals of power electronics* (2nd ed., p. 2). Kluwer Academic Publishers. http://site.ebrary.com/lib/nankai/Doc?id=10067440&page=25
[32] Poco EDM Technical Manual. (n.d.). *Chapter 3: Controlling the Spark* [Web page]. Retrieved September 4, 2025, from Poco EDM Technical Manual website: https://www.edmtechman.com/about.cfm?chap=3&pg=2
[33] Done.land. (2024). *XL4015 voltage regulator*. DONE.LAND. Retrieved September 1, 2025. https://done.land/components/power/powersupplies/dc-dc-converters/xl4015/